Generation of coherently coupled vibronic oscillations in carotenoids

Mitsuru Sugisaki,[1,2,3,*] Daisuke Kosumi,[1,2] Keisuke Saito,[2,3] Richard J. Cogdell,[4] and Hideki Hashimoto[1,2,3]

[1]*Graduate School of Science, Osaka City University, 3-3-138 Sugimoto, Sumiyoshi, Osaka 558-8585, Japan*

[2]*CREST-JST, K's Gobancho 6F, Chiyoda, Tokyo 102-0076, Japan*

[3]*OCARINA-OCU, Osaka 558-8585, Japan*

[4]*Institute of Molecular, Cell and Systems Biology, College of Medical, Veterinary and Life Sciences, University of Glasgow, Glasgow G12 8QQ, Scotland, United Kingdom*

(Received 23 December 2010; revised manuscript received 19 October 2011; published 5 June 2012)

Coherent vibronic oscillations in the ground state of carotenoids have been investigated by means of three-pulse four-wave mixing spectroscopy. Here, we especially focused our attention on the influence of the temporal separation between the first and the second pulses, i.e., the coherent period τ, on the third-order nonlinear signals. The vibronic oscillations of the fundamental modes are clearly observed when τ is set to zero. They appear via an impulsive resonant Raman process and reflect the spectral feature of a conventional Raman spectrum very well. Interestingly, in addition to the coherent vibronic oscillations of the fundamental modes, we found that high-intensity coherent vibronic oscillations of the overtones and the coupled modes appear when a nonzero value of τ is employed. These coupled modes become dominant at a rather large coherent period of $\tau \sim 60$ fs. A simple extension of our previous calculations that assume electronic harmonic potentials and vibronic Brownian oscillators cannot explain the present experimental results. Instead, we propose a model that takes into consideration the mixing between singlet states and the higher-order interaction of molecular vibrations with electronic states, which is in quantitative agreement with the experimental results. Our finding opens the way to controlling even Raman *inactive* vibronic oscillations using light.

DOI: 10.1103/PhysRevB.85.245408 PACS number(s): 82.53.Ps, 42.65.−k, 63.22.−m, 78.20.Bh

I. INTRODUCTION

The past decades have witnessed considerable progress in ultrashort laser technology, which has made it possible to observe the molecular vibronic oscillations in real time.[1] Recently, much attention has been devoted to observing these real-time vibronic oscillations because they provide us with rich information on the electronic and vibronic structures beyond static measurements (see, for example, Refs. 2 and 3). Another important aspect of coherent vibronic motions is their potential application in controlling the properties of materials, such as energy flow, isomerization, and so on.[4,5] Studies on coherent vibronic oscillations have so far been focused mainly on the fundamental vibronic modes that are IR and/or Raman active; these modes have already been well recognized. However, it is interesting to identify new methods to efficiently activate other modes that are, for example, Raman and IR inactive, because these modes, which include overtones and coupled modes, may reveal interesting aspects of materials and may enable us to extract their novel functions via, for example, biomolecular reactions, bond-selected reactions, and the control of vibrational energy flow.[6,7] These methodologies and techniques are based on the idea that driving an efficient reaction to form a specific product over others requires the excitation of vibrations that preferentially couple to a specific motion along the desired reaction coordinate.[8] The precise coherent control of higher vibronic modes is also required for application as multiple qubits for quantum computation.[9] Furthermore, it has been reported that the enhancement or suppression of the excitation energy flow during the early stages of photosynthesis is related to the excitation of a fundamental mode,[4] although the involvement of overtones and coupled modes is still not clear. Therefore, the development of new methodologies capable of exciting such modes on demand is interesting.

The excitation of vibronic oscillations via the Raman process is well described by the selection rule. For molecules that have harmonic potentials, this selection rule requires the satisfaction of the well-known relationship: The initial nth vibrational level is related with the final mth vibrational level by $m = n \pm 1$.[10] This means that only the fundamental modes can be observed in the Raman spectrum. In other words, the overtones and the combination processes by two vibronic modes are Raman forbidden. This relationship is relaxed when the molecular potential deviates from the simple harmonic model, for example, because of anharmonicity and the Duschinsky rotation.[10,11] Consequently, the overtones and coupled modes can be observed in the Raman spectra in these cases.

The excitation of the coupled modes can be obtained relatively easily when the molecular Raman spectra are measured under the photoexcitations that are much greater than their fundamental absorption edge because of vibronic coupling and the non-negligible anharmonicity of the potential shape. Nonetheless, despite the relaxation of the selection rule $m = n \pm 1$, the strongest resonance Raman-scattering peaks usually reflect transitions where the quantum number of a particular vibrational mode goes from 0 to 1, namely, the fundamental modes.[10] In addition, the photoexcitation at very high energy is not always preferable especially for organic molecules because the excess energy sometimes results in the degradation or even destruction of the sample molecules themselves. Therefore, it is necessary to explore other methodologies to efficiently generate coupled modes under the photoexcitation in the vicinity of or below the absorption edge.

The suppression of both the fundamental and the coupled modes has been demonstrated using optical pulses where the spectral chirp and shape are properly designed.[7,12] Although the enhancement of fundamental modes has also been observed,[13] it is not easy to significantly enhance the coupled

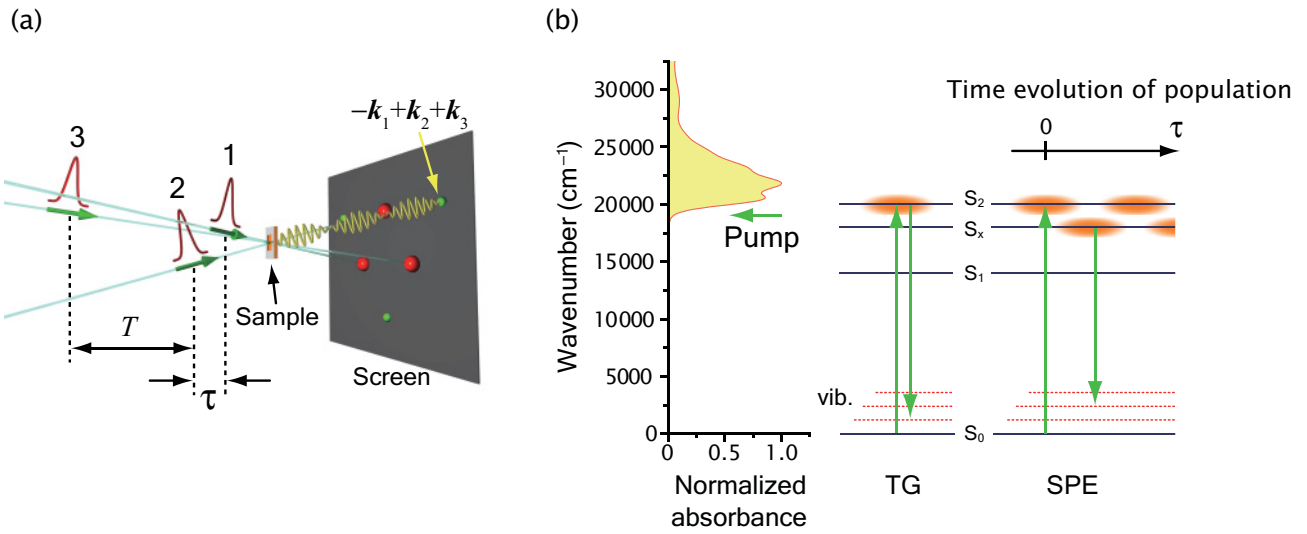

FIG. 1. (Color online) (a) The pulse sequence and the resulting FWM signals (small spots on the screen) that appear along the phase-matching directions, e.g., $-\boldsymbol{k}_1 + \boldsymbol{k}_2 + \boldsymbol{k}_3$, where $\boldsymbol{k}_i$ ($i = 1, 2, 3$) indicates the momentum vector of the ith pump pulse. (b) The linear absorption spectrum of β-carotene and its energy diagram with the ground-state vibronic levels. Carotenoids have a characteristic strong absorption in the visible region, which is the result of electronic transitions from their ground state S_0 to the higher excited singlet state S_2. One-photon transitions between the ground state and the first excited singlet state S_1 are symmetry forbidden. For the analysis of the FWM signals, we took a coherent interaction between S_2 and an intermediate state S_x into consideration. The complete set of energy diagrams used for the calculation can be found in Ref. 17. The periodic gradation on the S_2 and S_x states represents the time evolution of the population: When these states are coupled, the population oscillates between these states due to the so-called quantum beat.

modes when the molecular potentials are harmonic. Specifically, the enhancement of coupled modes is not expected simply by the use of a chirped pulse because the parity of the photons cannot be changed even if a pulse is spectrally chirped, which does not cause a breakdown in the Raman selection rule. Therefore, not only the control of the amplitudes of the overtones and coupled modes, but also the efficient excitation of such modes are, in themselves, not easy tasks to achieve.

In this paper, we report strong coherent couplings among vibronic oscillations observed in the four-wave mixing (FWM) signals from carotenoids, which are pigments abundantly present in nature that play important roles in the initial steps of photosynthesis.[14,15] The photoexcitation was performed at the absorption edge of carotenoids using sub-20-fs pulses. The coupling and decoupling of vibronic modes can be achieved on demand simply by controlling the temporal separation of the pump pulses. This experimental result can be explained by the coherent coupling of electronic excited states. We also comment on possible extensions of our findings to other materials.

II. EXPERIMENTAL DETAILS

β-carotene was purchased from Wako Pure Chemical Industries, Ltd. and was purified by recrystallization from a benzene solution. For the optical measurements, β-carotene was dissolved in tetrahydrofuran (THF). The concentration of the sample was adjusted to an optical density of $\sim$1 at its absorption maximum. All optical measurements were performed at room temperature.

As the excitation light source for the optical measurements, we constructed a noncollinear optical parametric amplifier (NOPA) using a femtosecond Ti:sapphire regenerative amplifier (Spectra-Physics, Hurricane).[16,17] The compressed output beam from the NOPA was divided into three using pellicle membranes with a thickness of 5 μm. The temporal separations between these pulses were controlled using linear-translation stages with a stepping resolution of 20 nm, which results in a temporal step of 0.13 fs (SIGMA TECH Co. Ltd., FS-1100PX). As schematically shown in Fig. 1(a), the pump pulses in the triangular configuration were focused onto the surface of a 100-μm-thick optical flow cell that was sandwiched between 1-mm-thick windows. The temporal widths of the pump pulses were optimized at the absorption edge as indicated in Fig. 1(b). For all the FWM measurements reported herein, the pulse widths measured using the cross-correlation technique were better than 16 fs.

Conventional Raman spectra excited using a continuous-wavelength laser at 532 nm were detected using a single monochromator (Acton Research, SpectraPro 306i) and a liquid-nitrogen-cooled charge-coupled-device camera (Roper Scientific, LN/CCD-1340/400-EB1). The spectral resolution of the system is better than 12 cm^{-1} over the whole spectral region examined. The concentration of the sample used for the Raman measurements was the same as that used during the FWM measurements.

III. RESULTS AND DISCUSSION

A. Temporal profile of FWM signals and conversion into the spectral domain

The FWM signals significantly depend on the temporal separations of the pulses [see the schematic in Fig. 1(a)]. One of the key parameters is the coherent period τ: The temporal separation between the first and the second pulses, where the polarizations induced by these pulses interfere in the sample.[18]

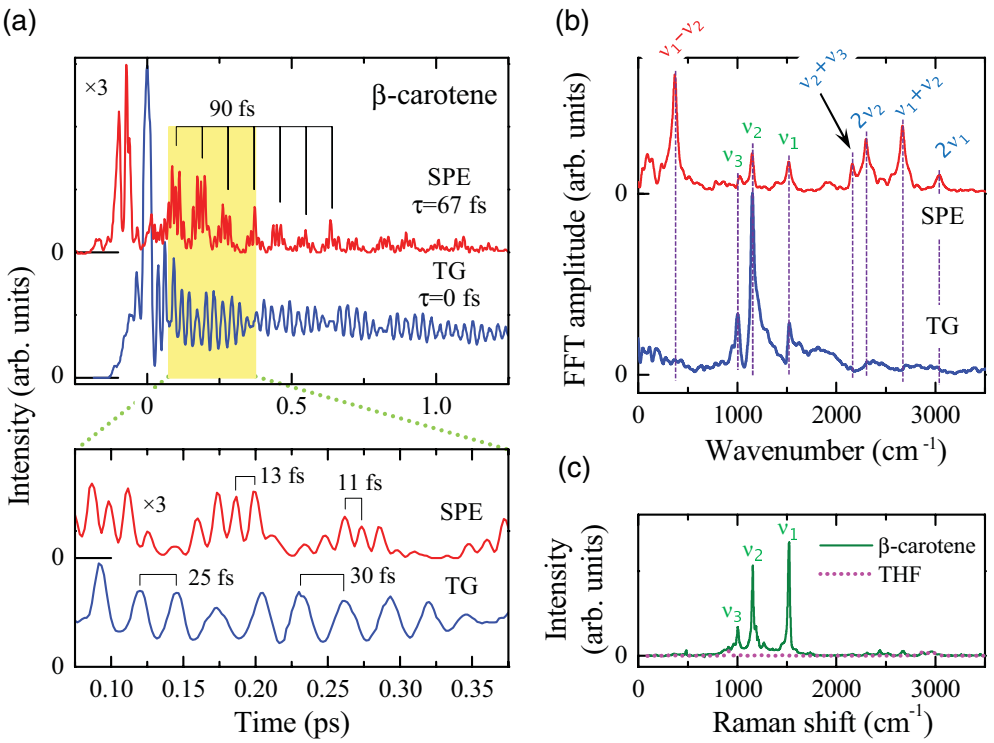

FIG. 2. (Color online) (a) The FWM signals in the TG and SPE configurations. The abscissa shows the population period T [the temporal separation between the second and third pulses; see Fig. 1(a)]. Magnified signals in the hatched area are shown in the lower panel. (b) Fourier-transformed spectra of the FWM signals. (c) The conventional Raman spectra of β-carotene and solvent (THF) for comparison. The dominant peaks at $\nu_1 = 1522$, $\nu_2 = 1157$, and $\nu_3 = 1004$ cm^{-1} are due to the symmetric stretching modes of the C=C and C—C bonds and the methyl-in-plane rocking mode in the ground state, respectively. In the time domain, these frequencies correspond to oscillation periods of 22.0, 28.9, and 33.2 fs, respectively.

The transient-grating (TG) signal from β-carotene in THF at $\tau = 0$ where the first and second pulses simultaneously excite the sample is shown in Fig. 2(a). Prominent coherent oscillations with a period of a few tens of femtoseconds are superimposed on a slowly decaying background, which reflects the electronic dynamics of internal conversion. The origin of the coherent oscillations seen in Fig. 2(a) can be readily understood by comparing the fast-Fourier-transform (FFT) spectrum [bottom curve in Fig. 2(b)] and the conventional Raman spectrum [Fig. 2(c)]. Namely, the peaks reflect the ground-state molecular vibronic oscillations.[12,16–20]

The temporal profile exhibits drastic changes when a nonzero value of τ is employed [the top curve of each panel in Fig. 2(a)], which is the so-called stimulated photon-echo (SPE) configuration. In this case, the slowly decaying background becomes very weak, but the coherent oscillations can still be clearly observed. Interestingly, the oscillation periods differ considerably from those measured in the TG configuration. The fast oscillations have a period of ~10 fs, which is approximately twice as fast as those in the TG configuration with an envelope of 90 fs. The FFT spectrum in the SPE configuration is shown in the top curve of Fig. 2(b).[21] In addition to the fundamental modes mentioned above, many new peaks were clearly observed both in the lower (0–500 cm^{-1}) and the higher (2000–3000 cm^{-1}) frequency regions. The energies of these distinct peaks agree quite well with the difference and sum of the fundamental modes. Thus, it can be concluded that these new peaks are coupled modes and overtones of the coherent vibronic oscillations.[20]

It should be emphasized that these coupled modes are inactive in the conventional Raman measurement [see Fig. 2(c)]. In general, because a Raman profile directly reflects the vibronic motions, it contains intrinsic information that can be used to characterize each molecule and is, therefore, sometimes called a fingerprint. The FFT spectrum in the TG configuration shows features comparable to the Raman spectrum. However, despite the smallness of the change in the experimental conditions, the FFT spectrum in the SPE configuration has a considerably different shape from its intrinsic fingerprint (Appendix A; see also the Supplemental Material[22]). To the best of our knowledge, such a significant intensity change between the fundamental and the coupled modes controlled by using ultrashort pulses has not been reported for any materials.

As shown in Fig. 3(a), the FWM measurement was repeated over a wide range of values for τ. When τ is less than 20 fs, the fundamental modes ν_1, ν_2, and ν_3 are dominant. The coupled modes, however, become dominant when τ is between 60 and 80 fs and are stronger than the fundamental modes. The fundamental modes and the coupled modes coexist with values of $\tau = 20$–60 fs. This result indicates that, despite the simplicity of this experimental technique, it is possible to excite higher-order vibronic oscillations on demand.[23]

In Fig. 3(b), the temporal changes in the coherent vibronic modes in the TG and SPE configurations are shown that are obtained by means of the wavelet analysis.[24] It is interesting

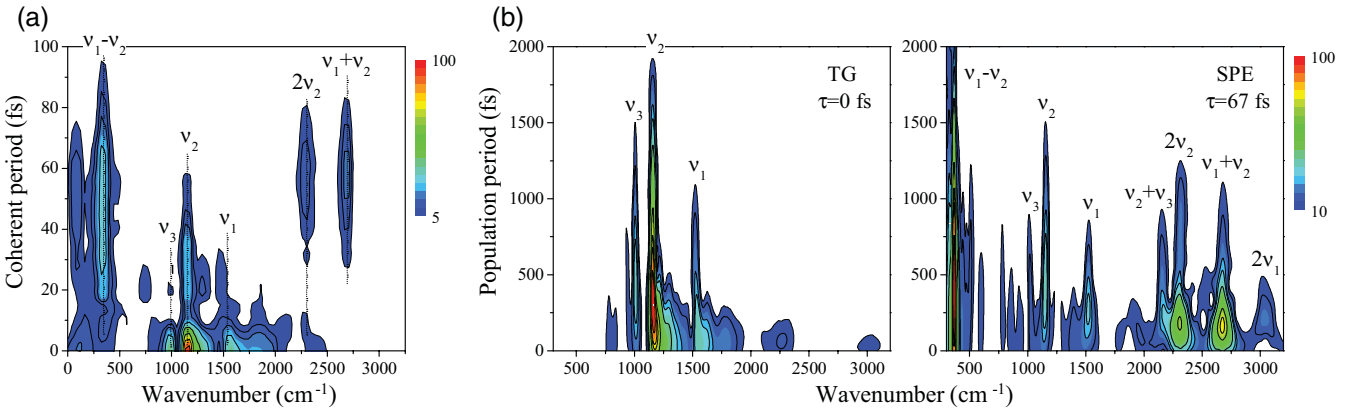

FIG. 3. (Color online) (a) A contour map showing the relative intensities of the coherent vibronic modes measured at various coherent periods. (b) Temporal changes in the coherent vibronic modes in the TG and SPE configurations. The coupled modes become very robust in the SPE configuration.

to note that the coupled modes that are excited in the SPE configuration are as robust as the fundamental modes, whereas, they are not observed as an intrinsic stable signal in Raman and IR measurements. Coupled modes have been previously observed for many materials, but they are usually very weak compared to the fundamental modes.[25] More importantly, the drastic change observed here in the relative intensity between the fundamental modes and the coupled modes is quite unusual.

It has been shown that the TG signals of carotenoids can be reproduced by calculating the third-order polarizability based on a multimode Brownian oscillator model.[16,17,26,27] An attempt was made to extend this type of calculation to the SPE data (Appendix B). However, this calculation resulted in amplitudes of the vibronic oscillations that were several orders of magnitude weaker than those observed in the experiment. Furthermore, the amplitudes of the coupled modes obtained during the calculation cannot become stronger than those of the fundamental modes. This fact indicates that a modification of the previous model is necessary in order to account for our findings. In the following, we discuss a possible model to explain the experimental results.

B. Model calculations and comparison with experimental results

We begin by describing the outline of our model. As explained in Introduction, the appearance of coupled modes in a Raman spectrum (or the FFT spectrum of a TG signal as in the present case) is due to the deviation from the simple harmonic potential model of the ground and/or excited states. However, in β-carotene, since the coupled modes in its Raman spectrum are very weak, both the ground state S_0 and the lowest optically allowed state S_2 are well approximated by harmonic potentials. Therefore, to explain the experimental result, it is, thus, necessary to introduce another electronic level that has anharmonicity or the Duschinsky rotation. Here, we ascribe this level to be the S_x state, which is located just below S_2 and is schematically depicted in Fig. 1(b). It should be noted that the possible existence of S_x is supported both theoretically and experimentally,[15] whereas, its potential shapes are still unknown. Furthermore, when the optically excited population in S_2 is stochastically relaxed to S_x, the coherent vibronic oscillations are also destroyed via this relaxation. However, the population in S_2 can get access to S_x without losing the initial coherence when the S_2 and S_x states are coherently coupled; therefore, coherent vibronic oscillations excited in the ground state are, thus, affected by the S_x state.[28]

We now describe more details of our calculation. The first key point is the introduction of the coupling between S_2 and S_x. The total Hamiltonian H of the system is given by

$$H = H_e + H_p + H_{ep} + H_{op}, \tag{1}$$

where H_e, H_p, H_{ep}, and H_{op} represent the Hamiltonians for the electron, the phonons (nuclear motion), the electron-phonon interactions, and the field-matter interactions, respectively. Because S_0, S_2, and S_x are involved immediately after the optical pumping, we can represent

$$H_e = \sum_{n=0,2,x} E_n|n\rangle\langle n| + V_{2x}|2\rangle\langle x| + \text{h.c.}, \tag{2}$$

where $|i\rangle$ indicates the S_i state with energy E_i and V_{2x} is the coupling constant between S_2 and S_x. By denoting the dipole moment between S_0 and S_2 as μ_{02}, we can write

$$H_{op} = \mu_{02}|0\rangle\langle 2|E\ \exp(i\omega_0 t) + \text{h.c.}, \tag{3}$$

where ω_0 and E are the angular frequency and amplitude of the incident photons, respectively.[26] The one-photon absorption process from S_0 to S_x is assumed to be negligible. Let us here assume that V_{2x} is not much larger than H_{op}, but the coherence between $|2\rangle$ and $|x\rangle$ is kept sufficiently long. In this situation, the first incident photon creates the optically allowed excited state $|2\rangle$. In the case of the TG configuration, because $|2\rangle$ created by the first photon is immediately dumped by the following second photon, $|x\rangle$ does not affect the signal. In contrast, in the case of the SPE configuration, because the transition from $|2\rangle$ to $|x\rangle$ is a coherent process rather than a stochastic process, the population oscillates between S_2 and S_x due to the so-called quantum beat until the second pulse arrives at the sample [see Fig. 1(b)].[26,29] Thus, the coherent vibronic oscillations in the ground state are affected by $|x\rangle$.

The second key point is an electron-phonon interaction, which has been introduced up to the second-order term, reflecting the observation of the coupled modes. For phonons, we can take

$$H_{\mathrm{p}} = \sum_{k} \frac{\hbar\omega_k}{2}\left(p_k^2 + q_k^2\right), \tag{4}$$

and

$$H_{\mathrm{ep}} = U_2(\boldsymbol{q})|2\rangle\langle 2| + U_{\mathrm{x}}(\boldsymbol{q})|\mathrm{x}\rangle\langle \mathrm{x}|, \tag{5}$$

where p_k and q_k represent the momentum and the coordinate, respectively, of the kth nuclear mode that has an angular frequency of ω_k.[26] Because only the fundamental modes appear in the observation from the TG signal that involves only $|2\rangle$, we can employ a simple linear interaction for S_2,[30]

$$U_2(\boldsymbol{q}) = \sum_{\mathrm{k}} \hbar\omega_k \eta_k q_k. \tag{6}$$

In contrast, because the coupled modes appear in the SPE signal that also involves $|\mathrm{x}\rangle$, a higher-order coupling term should be assumed for S_{x},

$$U_{\mathrm{x}}(\boldsymbol{q}) = \sum_{k} \hbar\omega_k \xi_k q_k + \sum_{kl} \hbar(\omega_k\omega_l)^{1/2}\chi_{kl} q_k q_l. \tag{7}$$

Here, η_i, ξ_i, and χ_{ij} represent the coupling strengths of the vibronic modes. Note that this mathematical expression of the second-order term gives a result that is consistent with the Duschinsky rotation.[2,11]

FWM signals can be calculated from the response functions that are pictorially represented by the Jablonski diagram and the double-sided Feynman diagrams.[26] The diagrams used in the present paper are the same as those used in our previous paper, which includes the excited singlet states S_1, S_{x}, S_2, and the higher states that are accessible from these states (see Fig. 5 in Ref. 17). However, in the present case, the coupling between S_2 and S_{x} has to be taken into consideration, which requires a modification of the response functions. Nonetheless, even in the presence of coherent coupling, the response functions can be described with a set of generally used response functions that are based on the four-point dipole correlation function[26] as described in Appendix C. Namely, when $V_{2\mathrm{x}}$ is not much larger than H_{op}, the response functions are still expressed by the original electronic basis set of $|0\rangle$, $|2\rangle$, and $|\mathrm{x}\rangle$ rather than by a basis set of the diagonalized eigenstates of H_{e}. We treat H_{ep} and H_{op} as the perturbation and describe a quantum interference effect of the quantum beat between $|2\rangle$ and $|\mathrm{x}\rangle$ by a linear combination of ordinary response functions expressed by the original basis. The higher-order interaction in H_{ep} has been approximated by the second-order cumulant expansion where the ordinary response functions can be expressed using the line-broadening function $g(t)$.

For simplicity, the energies of the S_2 and S_{x} states are set to be $E_2 = E_{\mathrm{x}} \equiv \hbar\omega_{\mathrm{r}}$ in the electronic Hamiltonian H_{e}. Suppose that the optically allowed state $|2\rangle$ is created from the electron-photon interaction H_{op} at time zero, i.e., $|2\mathrm{x}(0)\rangle = |2\rangle$. The electronic state at time t is denoted as $|2\mathrm{x}(t)\rangle$, where $|2\mathrm{x}\rangle$ stands for the mixing of $|2\rangle$ and $|\mathrm{x}\rangle$. In the coherent limit,

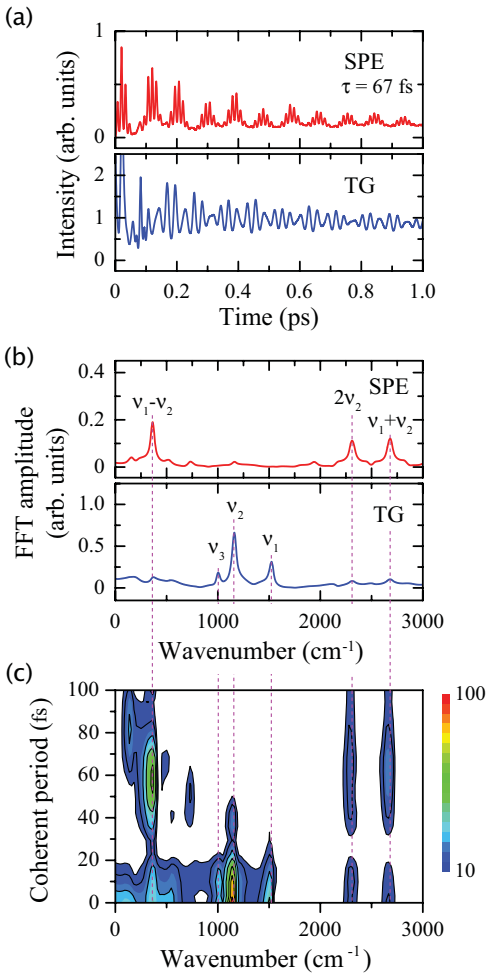

FIG. 4. (Color online) (a) Calculated FWM signals in the TG and SPE configurations and (b) their FFT spectra, which reproduce the experimental results shown in Figs. 2(a) and 2(b), respectively. (c) Relative intensities of the fundamental and coupled vibronic modes calculated at various values of τ. The agreement with the experimental result shown in Fig. 3(a) is quite good.

the temporal evolution of $|2\mathrm{x}\rangle$ is given by diagonalizing H_{e},

$$|2\mathrm{x}(t)\rangle = \frac{1}{\sqrt{2}} e^{-i\omega_{\mathrm{r}}t}\left(e^{-i\Delta\omega t}|+\rangle + e^{i\Delta\omega t}|-\rangle\right), \tag{8}$$

with the half-difference $\hbar\Delta\omega \equiv V_{2\mathrm{x}}$ between the eigenenergies and

$$|\pm\rangle \equiv \frac{1}{\sqrt{2}}(|2\rangle \pm |\mathrm{x}\rangle). \tag{9}$$

This time evolution represents the quantum beat between $|2\rangle$ and $|\mathrm{x}\rangle$ due to the coherent coupling $V_{2\mathrm{x}}$. As shown in Appendix C, our response functions, including the quantum-beat effect, can be expressed with $|2\mathrm{x}(t)\rangle$.

Figure 4 shows the results of the model calculation described above. The experimental results are satisfactorily reproduced when the following parameters are used to simulate the signals and spectra: $V_{2\mathrm{x}} = 100\ \mathrm{cm}^{-1}$, $\eta_1 = 0.4$, $\eta_2 = 0.5$, $\eta_3 = 0.2$, $\chi_{12} = 0.2$, $\chi_{22} = 0.2$, and $\xi_i = 0$. These calculations illustrate that the coupled modes and overtones are dominant in the SPE configuration, whereas, only the fundamental modes are observed in the TG configuration. The close agreement

between the experimental results and the calculations supports the validity of the extended model we employed; we conclude that the appearance of the coupled modes and the overtones is due to the coherent coupling between the excited states S_2 and S_x and the electron-phonon interaction.

IV. SUMMARY

We have observed the strong coupling between the coherent vibronic oscillations of β-carotene in an organic solvent by means of the FWM spectroscopy. The strength of such a coupling is controllable simply by tuning the temporal separation of pump pulses. Notably, when the coherent period τ is set to a moderate time, the coupled modes become stronger than the fundamental modes, which cannot be explained by the simple Raman selection rule that is successfully applied for molecules having harmonic vibrational modes, although the conventional resonance Raman-scattering and TG measurements clearly indicate that β-carotene has harmonic potentials. Since the numerical calculation that uses the widely accepted model could not reproduce our experimental results, additional effects have been taken into consideration, i.e., a coupling between the S_2 and the S_x states and an electron-phonon interaction that includes the influence of the Duschinsky rotation. It was found that this model significantly improves the agreement with the experimental results. Future papers for determining the most realistic potential curves of the electronic states of carotenoids will help better understand our results. It should be noted once again that the model proposed in the present paper is a plausible interpretation of the experiment. Other possible model calculations are also an important subject for future study.

Finally, we comment on the important points revealed in the present paper. The existence of the intermediate states between S_1 and S_2 has been discussed by many authors because the efficiency and pathways of energy transfer in photosynthesis involving carotenoids depend significantly on such states.[15] The experimental results and model calculations presented here also support the existence of an intermediate state, but more importantly, these results show that this state is coherently coupled to S_2.[28] In addition, because the key requirement of our model is the existence of coherently coupled electronic states, the enhanced coupling between vibronic modes will be possible not only in organic molecules, but also in other functional systems, such as in inorganic semiconductor quantum structures in which the coupling between electronic states is controllable in an external field.[31] By properly designing their electronic and phonon structures, coupled modes may be used, for example, to tailor the spectral range of coherent phonons.[32]

ACKNOWLEDGMENTS

The authors would like to thank Dr. S. V. Nair for providing source codes to calculate SPE signals and for helpful discussions. This work was supported by a Grant-in-Aid from the Japanese Ministry of Education, Culture, Sports, Science, and Technology (Grants No. 22340085, No. 22740276, and No. 23654151). R.J.C. acknowledges funding by the BBSRC. H.H. thanks the Nissan Science Foundation and HFSP for their financial support.

APPENDIX A: AMPLITUDE OF VIBRONIC OSCILLATIONS AT VARIOUS τ'S

The vibronic modes excited in the TG and SPE configurations show quite different features, which can be easily seen in the FFT spectra. To help demonstrate the significance of these differences, we provide Supplemental Material (the figures used in the Supplemental Material are also shown in Fig. 5).[22] The Supplemental Material represents the change in the coherent vibronic oscillations as changes in sound. Here, to shift the frequencies of all the vibronic modes observed in the experiments into an audible range for our ears, the most intense peak in the TG configuration ν_2 was normalized at 440 Hz. The relative intensities of each sound mode are shown in the lower panels. The later scenes of the Supplemental Material also demonstrate the coherent time dependence in a similar way.

Electronic structures and vibronic oscillations (or phonons) are the most fundamental and intrinsic characteristics that can definitively distinguish materials from one another. The control of functional materials using light has attracted considerable attention in recent years.[33] For materials showing a photoinduced phase transition or photochromism, a change in "color" is sometimes observed upon photoirradiation. In contrast, the present result can be intuitively understood as a change in "sound" upon photoirradiation. In this regard, it is interesting to note that real-time motion of acoustic phonons has been observed in the third-order optical responses from semiconductor quantum wells and superlattices.[34] Therefore, our experimental results suggest that sound control by light should be possible, in principle.

APPENDIX B: CALCULATION USING THE PREVIOUS MODEL

Figure 6 shows a series of FFT spectra of FWM signals in the impulsive limit calculated using the method reported in Refs. 16, 17, and 27. To include the influence of the temporal width of the excitation pulses, the spectral density is scaled. This model reproduced the experimental result of the TG signal, i.e., the fundamental modes ν_1, ν_2, and ν_3 appear clearly at $\tau = 0$. Here, we simply extended this model to the SPE regions, i.e., nonzero values of τ are introduced for the calculation. With the increase in the coherent period, new peaks due to the coherent coupling between the vibronic oscillations are observed, which is qualitatively consistent with our experimental results. Namely, even when the previous model is used, the coupled modes appear in the SPE configuration. However, the calculated results contain fatal quantitative inconsistencies with the experimental data. For example, the coupled modes are dominant around $\tau =$ 60 fs in the experiment, whereas, those in the calculations are maximal around $\tau =$ 10–20 fs. Furthermore, because the SPE signal monotonically decreased in intensity as τ increased, the amplitude of the calculated FFT spectrum around $\tau =$ 60 fs was several orders of magnitude weaker than what we observed. We have repeated the calculations by changing the parameters but could not reproduce the experimental results quantitatively.

In all of the calculated spectra shown in Fig. 6, the intensities of the coupled mode were always weaker than those

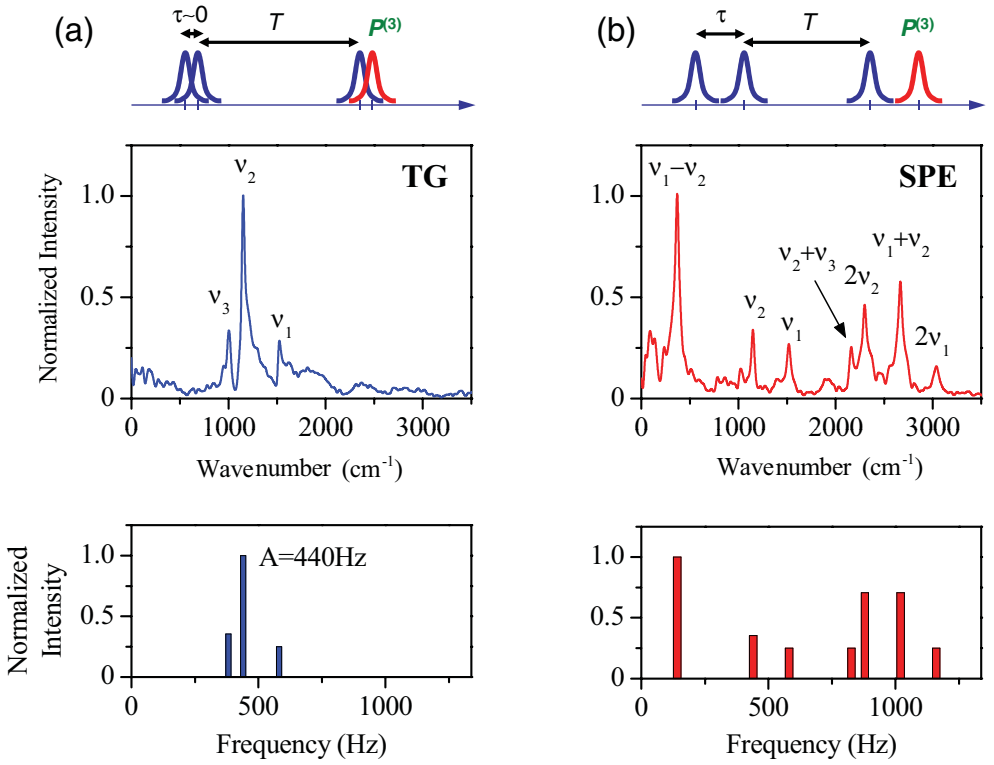

FIG. 5. (Color online) Figures used in the Supplemental Material.[22] The pulse sequences for the TG and SPE configurations are shown in the upper panels. The panels in the middle row show the FFT spectra of the FWM signals shown in Fig. 2(b). The relative amplitudes of the sound modes in the video file are shown in the lower panels.

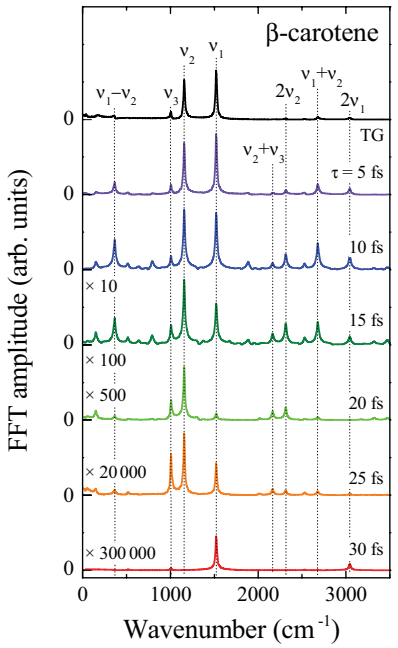

FIG. 6. (Color online) Numerically calculated FFT spectra of FWM signals in the impulsive limit. The numbers on the right indicate the coherent periods τ. In addition to the fundamental modes, the coupled modes appear at around 10–20 fs. However, the FFT amplitudes and the coherent period at which the coupled modes appear are much smaller than the experimental results.

of the fundamental modes. The failure in this calculation is caused by the following reason: When a linear interaction is simply taken into consideration as in the previous model, the coupled modes appear as the higher-order terms of the exponential expansion,[26]

$$R_i \propto A_{\rm bg} \exp[B_{\rm osc}] = A_{\rm bg}\left[1 + B_{\rm osc} + \tfrac{1}{2}B_{\rm osc}^2 + \cdots\right], \quad \text{(B1)}$$

where $A_{\rm bg}$ and $B_{\rm osc}$ indicate the amplitude and vibronic oscillations of the response functions R_i. Here, the second and third terms on the right-hand side give the fundamental and the second-order coupled modes, respectively, in the FWM signals. The oscillational term $B_{\rm osc}$ can be described as

$$B_{\rm osc} = \sum_n S_n C_n, \quad \text{(B2)}$$

with

$$C_n = \coth\left(\frac{\hbar\omega_n}{k_{\rm B}T}\right)(1 - \cos\omega_n t) + i\sin\omega_n t, \quad \text{(B3)}$$

where ω_n and S_n represent the angular frequency and the Huang-Rhys factor for the nth vibrational mode. Since $\hbar\omega_n \gg k_{\rm B}T$ and $S_n <\sim 1$ for a typical intramolecular vibration, the magnitude of each component C_n in $B_{\rm osc}$ is smaller than unity. Therefore, as can be understood from the coefficients of $B_{\rm osc}$ in Eq. (B1), the coupled modes $B_{\rm osc}^2$ (coefficient = 1/2) never become stronger than the fundamental mode $B_{\rm osc}$

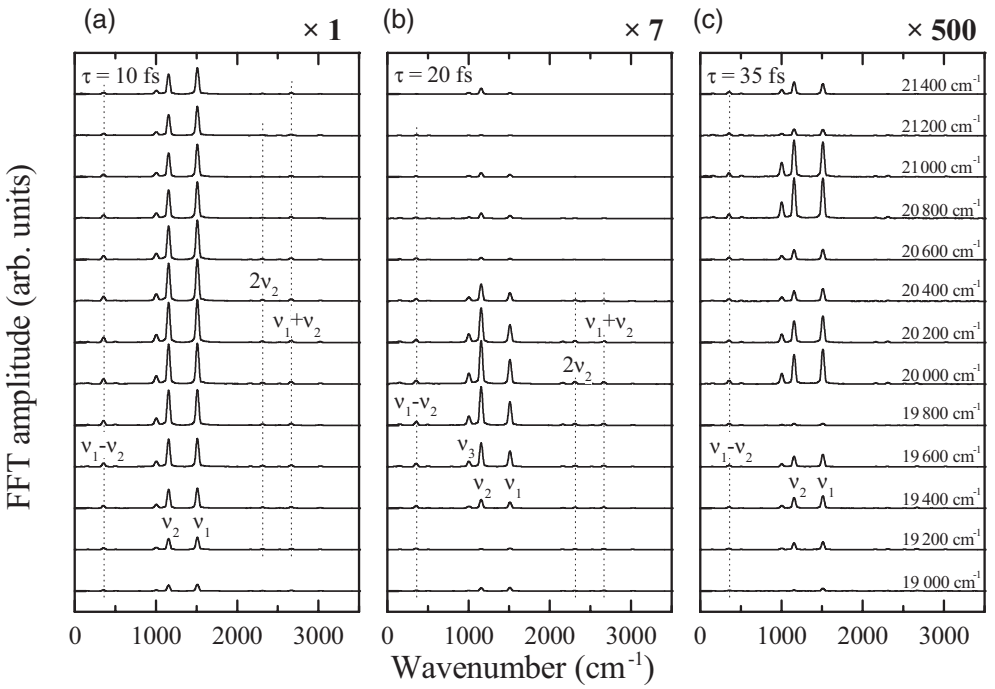

FIG. 7. FFT spectra calculated at various excitation energies and coherent periods. The pulse width is assumed to be 10 fs. The other parameters used for the calculations are the same as those used in Ref. 17. In all the cases, the coupled modes are much weaker than the fundamental modes. With the increase in the coherent period τ, the FFT amplitudes of the spectra decrease drastically. The curves in panels (b) and (c) are, respectively, magnified 7 and 500 times for clarity.

(coefficient = 1) when only a linear interaction is taken into account, whereas, the coupled modes are much stronger than the fundamental modes in the experiment.

The FFT spectra were also calculated at various excitation energies as shown in Fig. 7. The details of this calculation have been reported in Ref. 17, but in the present case, the calculations at various τ's were performed to determine the influence of a spectral chirp of pump pulses. Bardeen *et al.* have reported that the cooling time of vibronic oscillations is significantly sensitive to the spectral chirp;[13] it is informative to see the relative intensities between the fundamental and the coupled modes by a numerical calculation. When pump pulses are chirped, an FFT spectrum of an FWM signal is produced from the sum of the FFT spectra at different coherent times and different energies.[35] As expected from the reports in Ref. 13, the enhancement and suppression of the fundamental modes are seen in Fig. 7. However, the coupled modes cannot become stronger than the fundamental modes, even when any combination of the FFT spectra is assumed.[10,36] In addition, the FFT amplitude becomes very weak, even at a small τ [see Fig. 7(c)]. Therefore, the spectral chirp of pump pulses cannot explain the strong coupled modes observed in the experiment. This outcome is readily understood because spectral chirp cannot change the parity of the dipole as described in Introduction: The Raman selection rule cannot be relaxed simply from the use of chirped pulses.

The discrepancies observed between the experiment and the calculation clearly indicate that an additional effect should be introduced to the model to fully explain the experimental data set. As explained in the main text, a possible model is to include the coherent coupling between S_2 and S_x and the electron-phonon interaction.

APPENDIX C: RESPONSE FUNCTION

We consider the response function for a Liouville pathway R_1 shown in Fig. 8 as a simple example, but the other response functions can be obtained in a similar manner. When the coupling V_{2x} is absent, the response function $R_1^{2,2}$ is simply depicted by the double-sided Feynman diagram with the template $R_1^{a,b}$ as shown in Fig. 8(a). On the other hand, when the coupling V_{2x} is present, the response function should be represented by $R_1^{2x,2x}$ where the time evolution by $|2\rangle$ in the pathway $R_1^{2,2}$ is replaced by $|2x(t)\rangle$ introduced in the main text. As shown in Fig. 8(b), by applying Eq. (8) to the time evolution $|2x(t)\rangle$ on the bra side in $R_1^{2x,2x}$, the response function for $R_1^{2x,2x}$ can be expressed as

$$R_1^{2x,2x}(\tau',T,\tau) = \frac{1}{\sqrt{2}}\left(e^{i\Delta\omega\tau}R_1^{2x,+} + e^{-i\Delta\omega\tau}R_1^{2x,-}\right). \quad \text{(C1)}$$

Here, the reference phase rotation by $\omega_r t$ is already included in $R_1^{2x,\pm}$, and the difference in the phase rotation by $\Delta\omega\tau$ is the inverse of that in Eq. (8) because of the bra side. Similarly, for the ket side of $R_1^{2x,\pm}$, we obtain

$$R_1^{2x,2x}(\tau',T,\tau) = \tfrac{1}{2}[e^{-i\Delta\omega(\tau'-\tau)}R_1^{+,+} + e^{-i\Delta\omega(\tau+\tau')}R_1^{+,-} + e^{i\Delta\omega(\tau'+\tau)}R_1^{-,+} + e^{i\Delta\omega(\tau'-\tau)}R_1^{-,-}]. \quad \text{(C2)}$$

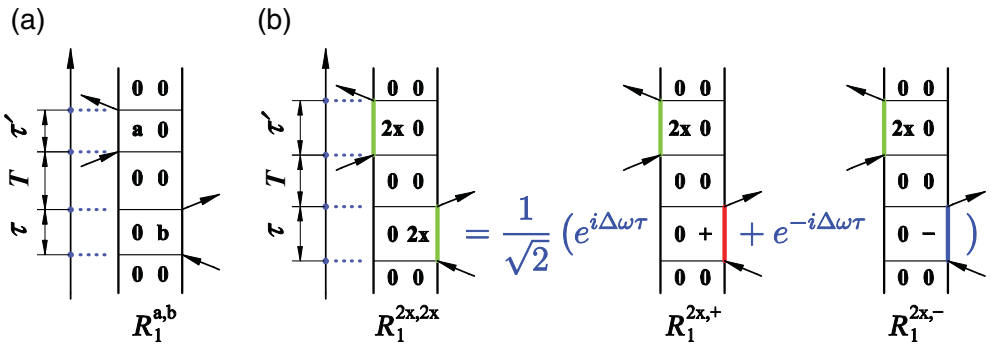

FIG. 8. (Color online) The double-sided Feynman diagrams for a pathway R_1. (a) Template of $R_1^{a,b}$ and (b) expression by the diagram for the response function of Eq. (C1).

From Eq. (9), $R_1^{\pm,\pm}$ can also be decomposed into

$$\begin{aligned} R_1^{+,+} &= \tfrac{1}{2}\big(R_1^{2,2} + R_1^{2,\mathrm{x}} + R_1^{\mathrm{x},2} + R_1^{\mathrm{x},\mathrm{x}}\big), \\ R_1^{+,-} &= \tfrac{1}{2}\big(R_1^{2,2} - R_1^{2,\mathrm{x}} + R_1^{\mathrm{x},2} - R_1^{\mathrm{x},\mathrm{x}}\big), \\ R_1^{-,+} &= \tfrac{1}{2}\big(R_1^{2,2} + R_1^{2,\mathrm{x}} - R_1^{\mathrm{x},2} - R_1^{\mathrm{x},\mathrm{x}}\big), \\ R_1^{-,-} &= \tfrac{1}{2}\big(R_1^{2,2} - R_1^{2,\mathrm{x}} - R_1^{\mathrm{x},2} + R_1^{\mathrm{x},\mathrm{x}}\big). \end{aligned} \tag{C3}$$

The response function $R_1^{2\mathrm{x},2\mathrm{x}}$ can, thus, be expressed by including the effect of coherent coupling $V_{2\mathrm{x}}$ in terms of elemental response functions $R_1^{2,2}$, $R_1^{2,\mathrm{x}}$, $R_1^{\mathrm{x},2}$, and $R_1^{\mathrm{x},\mathrm{x}}$ described by the original electronic states $|2\rangle$ and $|\mathrm{x}\rangle$ without the coupling.

The elemental response functions, appearing in Eq. (C3), can be readily calculated by means of the second-order cumulant expansion.[26] Here, we note that the cumulant expansion of the higher-order interaction includes not only second-order cumulants, but also even higher-order cumulants. However, it is generally expected that the term becomes less effective as the order of the cumulant increases. Therefore, we truncated at the second order, and the higher-order terms are approximated to be negligibly small.[37] In this approximation, we can express the elemental response functions as

$$\begin{aligned} R_1^{a,b}(\tau',T,\tau) = \exp[i\tau\omega_b - i\tau'\omega_a]\exp[&-g_{bb}^*(\tau) + g_{ab}^*(T) \\ &- g_{aa}(\tau') - g_{ab}^*(\tau+T) - g_{ab}^*(T+\tau') \\ &+ g_{ab}^*(\tau+T+\tau')]. \end{aligned} \tag{C4}$$

Here, $g_{ab}(t)$ represents the line-broadening function,

$$g_{ab}(t) = \frac{1}{\hbar^2}\int_0^t dt_1 \int_0^{t_1} dt_2 \langle \bar{U}_a(\boldsymbol{q};t_2)\bar{U}_b(\boldsymbol{q};0)\rangle, \tag{C5}$$

with the zero-averaged interaction $\bar{U}_a(\boldsymbol{q}) \equiv U_a(\boldsymbol{q}) - \langle U_a(\boldsymbol{q})\rangle$ and its Heisenberg picture $U_a(\boldsymbol{q};t) \equiv e^{iH_\mathrm{p}t/\hbar}U_a(\boldsymbol{q})e^{-iH_\mathrm{p}t/\hbar}$. The thermal average is defined as $\langle\cdots\rangle \equiv \mathrm{Tr}[\rho_\mathrm{eq}\cdots]$ with $\rho_\mathrm{eq} \equiv e^{-\beta H_\mathrm{p}}/\mathrm{Tr}[e^{-\beta H_\mathrm{p}}]$, where β is the inverse temperature $(k_\mathrm{B}T)^{-1}$ and Tr means taking the trace on the vibronic degrees. The frequency ω_a is defined by $\hbar\omega_a \equiv E_a - E_0 + \langle U_a(\boldsymbol{q})\rangle$. The correlation function $\langle \bar{U}_a(\boldsymbol{q};t_2)\bar{U}_b(\boldsymbol{q};0)\rangle$ in Eq. (C5) can be calculated by a straightforward extension of the method shown in Ref. 26. This correlation function eventually includes the coupling mode originating from the second-order term in Eq. (7).

*Corresponding author: mitsuru@sci.osaka-cu.ac.jp

[1] S. De Silvestri, G. Cerullo, and G. Lanzani, *Coherent Vibrational Dynamics* (CRC, Boca Raton/London/New York, 2007).

[2] T. Fuji, T. Saito, and T. Kobayashi, Chem. Phys. Lett. **332**, 324 (2000).

[3] L. Lüer, C. Gadermaier, J. Crochet, T. Hertel, D. Brida, and G. Lanzani, Phys. Rev. Lett. **102**, 127401 (2009); Y. Kawakami, T. Fukatsu, Y. Sakurai, H. Unno, H. Itoh, S. Iwai, T. Sasaki, K. Yamamoto, K. Yakushi, and K. Yonemitsu, *ibid.* **105**, 246402 (2010)

[4] J. L. Herek, W. Wohlleben, R. J. Cogdell, D. Zeidler, and M. Motzkus, Nature (London) **417**, 533 (2002); W. Wohlleben, T. Buckup, J. L. Herek, and M. Motzkus, Chem. Phys. Chem. **6**, 850 (2005); J. Savolainen, R. Fanciulli, N. Dijkhuizen, A. L. Moore, J. Hauer, T. Buckup, M. Motzkus, and J. L. Herek, Proc. Natl. Acad. Sci. USA **105**, 7641 (2008).

[5] V. I. Prokhorenko, A. M. Nagy, S. A. Waschuk, L. S. Brown, R. R. Birge, and R. J. D. Miller, Science **313**, 1257 (2006).

[6] A. M. Weiner, D. E. Leaird, G. P. Wiederrecht, and K. A. Nelson, Science **247**, 1317 (1990); T. C. Weinacht, J. L. White, and P. H. Bucksbaum, J. Phys. Chem. A **103**, 10166 (1999); M. Gruebele and P. G. Wolynes, Acc. Chem. Res. **37**, 261 (2004); D. R. Killelea, V. L. Campbell, N. S. Shuman, and A. L. Utz, Science **319**, 790 (2008); Y. Zhang, H. Fujisaki, and J. E. Straub, J. Chem. Phys. **130**, 025102 (2009); Y. Zhang and J. E. Straub, *ibid.* **130**, 095102 (2009); **130**, 3147704 (2009).

[7] R. A. Bartels, T. C. Weinacht, S. R. Leone, H. C. Kapteyn, and M. M. Murnane, Phys. Rev. Lett. **88**, 033001 (2002).

[8] P. Kukura, D. W. McCamant, S. Yoon, D. B. Wandschneider, and R. A. Mathies, Science **310**, 1006 (2005); S. Yoon, R. J. Holiday, and F. F. Crim, J. Phys. Chem. B **109**, 8388 (2005).

[9] M. Tsubouchi and T. Momose, Phys. Rev. A **77**, 052326 (2008).

[10] W. W. Parson, *Modern Optical Spectroscopy: With Examples from Biophysics and Biochemistry* (Springer-Verlag, Berlin, 2006).

[11] F. Duschinsky, Acta Physicochim URSS **7**, 551 (1937); F. Santoro, C. Cappelli, and V. Barone, J. Chem. Theory Comput. **7**, 1824 (2011); I. Özkan, J. Mol. Spectrosc. **139**, 147 (1990); G. M. Sando, K. G. Spears, J. T. Hupp, and P. T. Ruhoff, J. Phys. Chem. A **105**, 5317 (2001).

[12]J. Konradi, A. K. Singh, A. V. Scaria, and A. Materny, J. Raman Spectrosc. **37**, 697 (2006); J. Hauer, H. Skenderovic, K. L. Kompa, and M. Motzkus, Chem. Phys. Lett. **421**, 523 (2006).

[13]C. J. Bardeen, Q. Wang, and C. V. Shank, Phys. Rev. Lett. **75**, 3410 (1995); J. Phys. Chem. A **102**, 2759 (1998).

[14]H. A. Frank and R. J. Cogdell, Photochem. Photobiol. **63**, 257 (1996).

[15]As review articles, T. Polívka and V. Sundström, Chem. Rev. **104**, 2021 (2004); Chem. Phys. Lett. **477**, 1 (2009).

[16]M. Sugisaki, K. Yanagi, R. J. Cogdell, and H. Hashimoto, Phys. Rev. B **75**, 155110 (2007).

[17]M. Sugisaki, M. Fujiwara, S. V. Nair, H. E. Ruda, R. J. Cogdell, and H. Hashimoto, Phys. Rev. B **80**, 035118 (2009).

[18]The relationship between the pulse sequences and the spectroscopic techniques is summarized in G. R. Fleming and M. Cho, Annu. Rev. Phys. Chem. **47**, 109 (1996); I. Pastirk, V. V. Lozovoy, and M. Dantus, Chem. Phys. Lett. **333**, 76 (2001); B. I. Grimberg, V. V. Lozovoy, M. Dantus, and S. Mukamel, J. Phys. Chem. **106**, 697 (2002).

[19]M. Fujiwara, K. Yamauchi, M. Sugisaki, K. Yanagi, A. Gall, B. Robert, R. J. Cogdell, and H. Hashimoto, Phys. Rev. B **78**, 161101 (2008); G. Cerullo, G. Lanzani, M. Zavelani-Rossi, and S. De Silvestri, *ibid.* **63**, 241104 (2001).

[20]S. Saito and M. Tasumi, J. Raman Spectrosc. **14**, 310 (1983); S. Saito, M. Tasumi, and C. H. Eugster, **14**, 299 (1983).

[21]The vibronic oscillations observed in the present paper are much stronger than those observed in Ref. 16. In addition to the better temporal width of the pulse obtained in the present paper, this difference is due to the stabilization of the experimental setup. This stabilization made it possible to clearly observe the vibronic oscillations even at large τ, i.e., up to $\tau \sim 100$ fs. However, the slowly varying background becomes very weak at only $\tau \sim 30$ fs, which is consistent with our previous paper.

[22]See Supplemental Material at http://link.aps.org/supplemental/10.1103/PhysRevB.85.245408 for a video representing the change in the coherent vibronic oscillations with the change in sound. The details of the coherent time dependence are demonstrated in the later scenes of the video file.

[23]We also measured the FWM signals using another carotenoid molecule, spheroidene. The results were consistent with those observed for β-carotene. Specifically, the fundamental modes that appear in the FFT spectrum of the TG signal are in good agreement with the Raman spectrum, and the coupled modes and the overtones can be observed in the SPE configuration. Therefore, we can conclude that the appearance of the coupled modes and the overtones in the SPE configuration is a common feature of carotenoids.

[24]M. Fujiwara, K. Yamauchi, M. Sugisaki, A. Gall, B. Robert, R. J. Cogdell, and H. Hashimoto, Phys. Rev. B **77**, 205118 (2008).

[25]See, for example, K. Ohta, D. S. Larsen, M. Yang, and G. R. Fleming, J. Chem. Phys. **114**, 8020 (2001); Y. Nagasawa, Y. Mori, Y. Nakagawa, H. Miyasuka, and T. Okada, J. Phys. Chem. B **109**, 11946 (2005); T. Kuroda, P. A. Zhokhov, K. Watanabe, A. M. Zheltikov, and K. Sakoda, Opt. Express **17**, 20794 (2009).

[26]S. Mukamel, *Principles of Nonlinear Optical Spectroscopy* (Oxford University Press, New York/Oxford, 1995).

[27]M. Sugisaki, M. Fujiwara, D. Kosumi, R. Fujii, M. Nango, R. J. Cogdell, and H. Hashimoto, Phys. Rev. B **81**, 245112 (2010).

[28]Recently, the coherent coupling between the singlet states in β-carotene has also been investigated by means of the pump-probe spectroscopy: J. L. P. Lustres *et al.*, Angew. Chem., Int. Ed. **46**, 3758 (2007); E. Ostroumov, M. G. Müller, C. M. Marian, M. Kleinschmidt, and A. R. Holzwarth, Phys. Rev. Lett. **103**, 108302 (2009); However, the interpretation of the experimental results is still under debate: N. Christensson *et al.*, J. Phys. Chem. Lett. **1**, 3366 (2010).

[29]R. W. Boyd, *Nonlinear Optics* (Academic, Amsterdam/Boston/Heidelberg, 2008).

[30]The model calculation was also performed by introducing the higher-order term for $U_2(\boldsymbol{q})$. However, in this case, the coupled modes appear even at $\tau = 0$, which is inconsistent with the experimental result.

[31]M. Bayer, P. Hawrylak, K. Hinzer, S. Fafard, M. Korkusinski, Z. R. Wasilewski, O. Stern, and A. Forchel, Science **291**, 451 (2001); E. A. Stinaff, M. Scheibner, A. S. Bracker, I. V. Ponomarev, V. L. Korenev, M. E. Ware, M. F. Doty, T. L. Reinecke, and D. Gammon, *ibid.* **311**, 636 (2006).

[32]J. Hebling, K. L. Yeh, M. C. Hoffmann, and K. A. Nelson, IEEE J. Sel. Top. Quantum Electron. **14**, 345 (2008); K. Mizoguchi, Y. Kanzawa, S. Saito, K. Sakai, and M. Nakayama, Appl. Phys. Lett. **94**, 171105 (2009).

[33]K. Nasu, *Photoinduced Phase Transitions* (World Scientific, Hackensack, NJ/London/Singapore/Beijing/Shanghai/Hong Kong/Taipei/Chennai 2004); M. Chollet, L. Guerin, N. Uchida, S. Fukaya, H. Shimoda, T. Ishikawa, K. Matsuda, T. Hasegawa, A. Ota, H. Yamochi, G. Saito, R. Tazaki, S. Adachi, and S. Koshihara, Science **307**, 86 (2005); T. Kobayashi, T. Saito, and H. Ohtani, Nature (London) **414**, 531 (2001); S. Ohkoshi, Y. Tsunobuchi, T. Matsuda, K. Hashimoto, A. Namai, F. Hakoe, and H. Tokoro, Nat. Chem. **2**, 539 (2010).

[34]A. Yamamoto, T. Mishina, Y. Masumoto, and M. Nakayama, Phys. Rev. Lett. **73**, 740 (1994); A. Bartels, T. Dekorsy, H. Kurz, and K. Köhler, *ibid.* **82**, 1044 (1999); Ü. Özgur, C.-W. Lee, and H. O. Everitt, *ibid.* **86**, 5604 (2001); Y. Ogawa, A. Iwamatsu, and F. Minami, Phys. Rev. B **73**, 153203 (2006); Y. Ogawa and F. Minami, *ibid.* **75**, 073302 (2007).

[35]In the present paper, the product of the spectral band width of pump pulse $\Delta\omega_p$ and pulse duration τ_p is 0.96. In other words, the pump pulses are wider by about 8 fs in comparison with the Fourier-limited case, which works as the chirp and gives the error bars of the coherent period.

[36]A. Wand, S. Kallush, O. Shoshanim, O. Bismuth, R. Kosloff, and S. Rhuman, PhysChemChemPhys **12**, 2149 (2010).

[37]If the higher-order cumulants were more important, the vibronic modes that are a combination of modes of third or higher order would be experimentally observed. This observation is not the case in the present paper.